Performance Evaluation and Loss Modeling of WBG Devices based on a Novel Double-Pulse Test Method for Current Source Inverter

Feida Chen Sangwhee Lee Renato A. Torres Thomas M. Jahns Bulent Sarlioglu
Wisconsin Electric Machines and Power Electronics Consortium (WEMPEC)
University of Wisconsin-Madison, WI 53706 USA
E-mail: *sarlioglu@ wisc.edu*

Abstract- **Careful measurements of the power device characteristics are necessary to accurately estimate a power converter's losses and efficiency. The conventional double-pulse test (DPT) circuit is a well-known method to implement this laboratory characterization of power devices and power modules. However, the switching characteristics of a power device depend on the power electronics circuit in which it is connected as well as the power circuit's physical layout, in addition to the device's internal structure. Hence, the conventional DPT circuit configuration, which is tailored for a standard voltage-source inverter (VSI), is not well-suited for a current-source inverter (CSI). This paper demonstrates a previously-proposed CSI-based DPT measurement technique that is appropriate for normal CSI operation. The characteristics of SiC MOSFETs and series-connected SiC Schottky diodes used in a CSI are measured using this improved technique while taking temperature effects into account to yield more accurate loss predictions. The CSI losses, including the switching and conduction losses of SiC MOSFETs and SiC Schottky diodes, have been modeled using this approach. The total CSI losses and efficiency have been estimated based on the CSI DPT results and loss models.**

Keywords **– Current-source inverter, double-pulse test, power loss, wide-bandgap devices, traction application**

I. INTRODUCTION

Wide-bandgap (WBG) power semiconductor devices that use either silicon carbide (SiC) or gallium nitride (GaN) are appealing for future motor drive systems due to their superior characteristics, including higher switching speeds, lower on-state resistance, and higher junction temperatures compared to conventional silicon (Si) devices [1-3]. However, there are some drawbacks in standard voltage-source inverters (VSIs) when conventional Si-based switches are replaced by WBG switches, including high electromagnetic interference (EMI), high motor terminal overvoltages, and damaging bearing current risks [4]. The emergence of wide-bandgap power devices opens opportunities for the long-ignored current-source inverter (CSI) to provide a promising alternative drive configuration for traction applications [5].

The basic CSI-based motor drive, including a dc/dc converter to provide the necessary input dc voltage-to-current conversion, is shown in Fig. 1. The CSI replaces the VSI's dc-link capacitor (<150 ºC) with a high-temperature dc-link inductor (>200 ºC) and three small output ac capacitors,

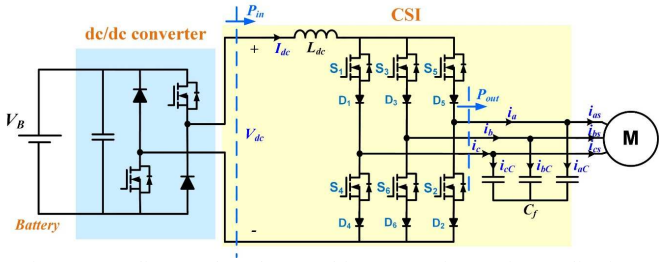

Fig. 1. Baseline CSI-based motor drive system for traction application

providing much more sinusoidal output voltage waveforms to the motor [5]. As shown in Fig. 1, SiC Schottky diodes are connected in series with the SiC MOSFETs to provide the reverse-voltage blocking capability for CSI. They will eventually be replaced by WBG monolithic bidirectional switches when they become commercially available [6]. In addition, the CSI has a natural voltage-boosting feature, which can be used to improve the overall efficiency of the CSI-based SPM machine drive system in the constant-power region [7].

To accurately evaluate the performance of WBG devices in the CSI, the conduction and switching characteristics of the power devices should be measured. The conventional double-pulse test (DPT) circuit used with standard VSIs is a well-known method to evaluate the transient performance metrics such as the turn-on/turn-off switching losses and the rise/fall time at different voltage and current levels. However, the switching characteristics of such devices are not only dependent on its internal structure, but also on the external circuit to which it is connected, including its physical layout.

In addition, the conventional DPT circuit configuration is not appropriate for testing the reverse-voltage blocking switches that are required in the CSI. Ding, et al. compared the characteristics of Si IGBTs and SiC MOSFETs using the VSI DPT circuit considering temperature effects [8]. Dai, et al examined the performance of WBG-based hybrid switches intended for CSIs using the conventional DPT circuit [9]. Nevertheless, few researchers have evaluated the device characteristics for CSI in its final circuit configuration.

A new DPT circuit topology, which is more suitable for CSIs, has been proposed by Torres, et al [10]. This paper presents the result of a project that has implemented this CSI-tailored DPT circuit to evaluate the performance of WBG

devices for use in a 55 kW (continuous) CSI. Power loss models for the SiC MOSFETs and SiC Schottky diodes used in this CSI have been developed based on the DPT results, including temperature effects.

This paper is organized as follows. Section II introduces and compares the conventional VSI-type DPT and the new DPT topology that is suitable for evaluating the characteristics of switches in CSI. In Section III, the characteristics of the SiC MOSFETs and SiC Schottky diodes are measured using the CSI DPT. In Section IV, the switching losses and conduction losses of the WBG devices are modeled based on the CSI DPT results, considering temperature effects. Concluding statements are presented in Section V.

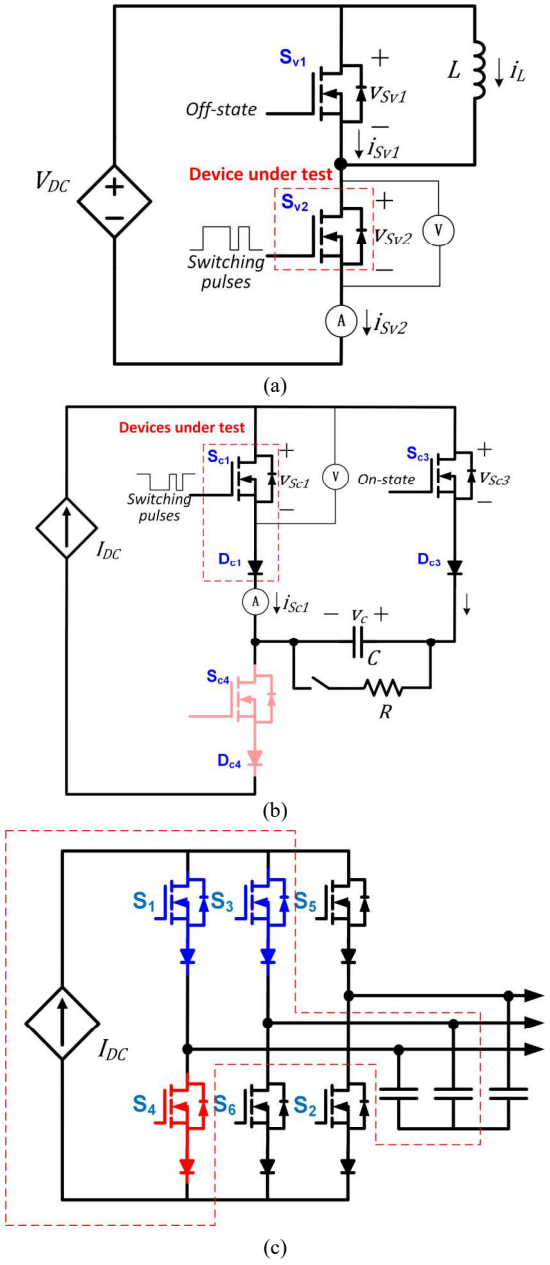

Fig. 2. (a) Conventional VSI DPT circuit; (b) Proposed CSI DPT circuit; (c) Basic 3-phase CSI topology (the dotted lines highlight the circuit paths that corresponds to the CSI DPT)

II. Double-Pulse Test for CSI

The VSI DPT and CSI DPT power circuit diagrams are very similar since both methods evaluate the switch state transition of a power device at a given current and voltage levels. The conventional VSI DPT is a simpler circuit topology to evaluate the switching performance of the power devices in VSI. However, the existing VSI DPT is not appropriate to measure reverse voltage blocking switches that are needed for CSI. In addition, since the external circuit layout can have a significant influence on the transient performance, and the topologies have different switch implementations, it is desirable to execute the DPT test using the circuit that corresponds to the adopted inverter topology. By taking this approach, the switching conditions will be as close as possible to the real operation of the current source inverter.

The conventional VSI DPT is well-known and shown in Fig. 2(a). The CSI DPT [10] is a dual topology of the conventional VSI DPT, as shown in Fig. 2(b). The operating principles of both of these circuits are explained in [10]. The voltage source in VSI DPT can be transformed into a current source in CSI DPT by replacing the inductor L of VSI DPT by a capacitor C for CSI DPT, and making the switches in the CSI DPT in parallel instead of switches in series in VSI DPT. An external resistor R with a switch is connected in parallel with the capacitor to discharge after the DPT operation for safety reasons. It can be observed from Fig. 2 (b) and (c), the CSI DPT is derived from the three-phase CSI topology. The switches S_{c1}, S_{c3} and S_{c4} in the CSI DPT represent S_1, S_3 and S_4 in the 3-phase CSI circuit. The CSI DPT corresponds to the commutation between S_1 and S_3 (blue in Fig. 2(c)) of the 3-phase CSI, where S_5, S_6 and S_2 are always off, and S_4 (red in Fig. 2(c)) is always on. The single output capacitor in CSI DPT is equivalent to the series-connected ac filter capacitor in the CSI during active states. It should be mentioned that as the switch S_4 of CSI is always ON at this special condition, and S_{c4} in the CSI DPT is replaced by a

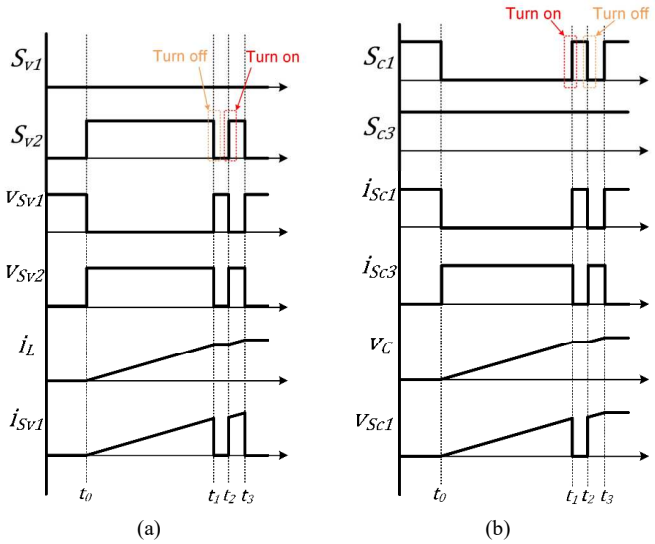

Fig. 3. (a) Typical VSI DPT waveforms; (b) CSI DPT waveforms;

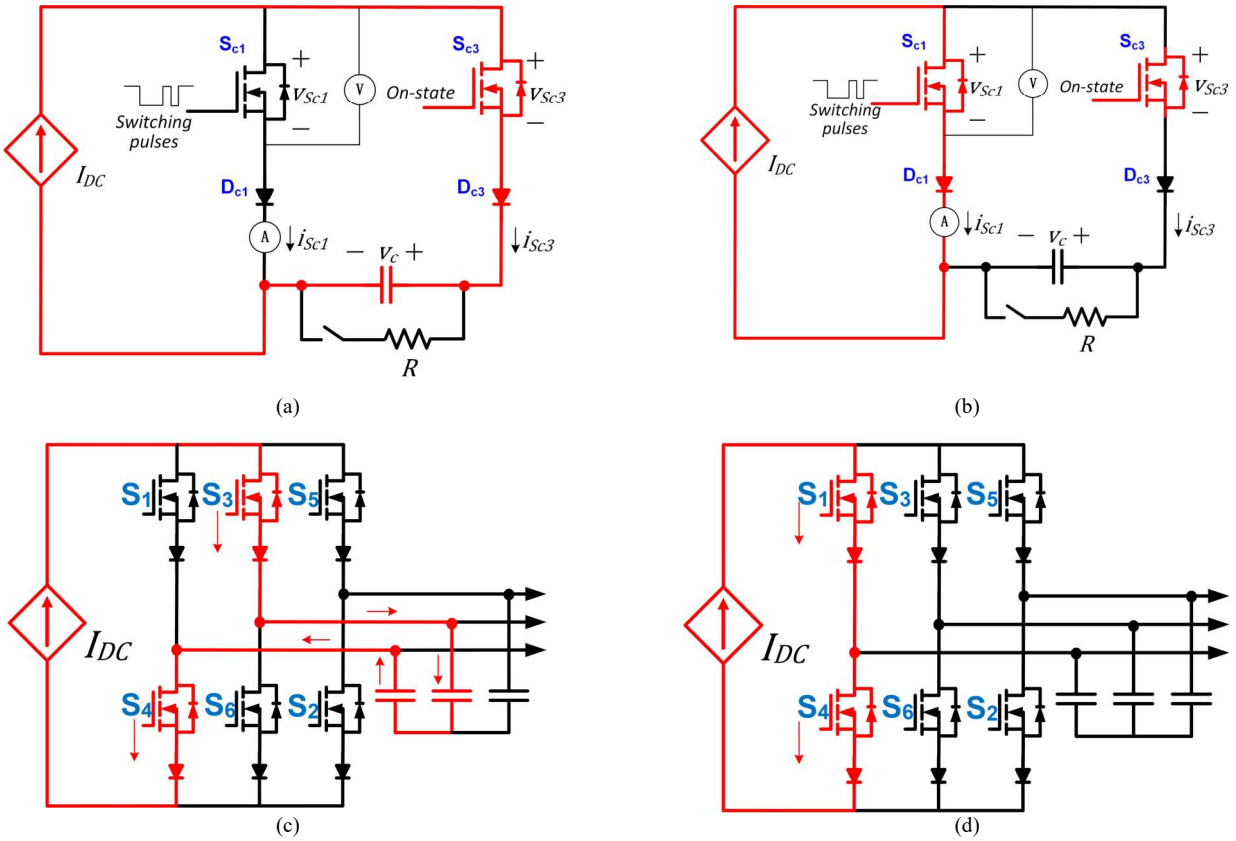

Fig. 4. (a) First condition when S_{c1} is turned off for CSI DPT; (b) Second condition when S_{c1} is turned on for CSI DPT; (c) Circuit paths of 3-phase CSI that correspond to first condition of CSI DPT (active state); (d) Circuit paths of 3-phase CSI that correspond to second condition of CSI DPT (zero state).

short circuit (ON state). This is shown in the CSI DPT circuit in Fig. 2b as grayed out to illustrate the fact that S_{c4} of CSI DPT corresponds to the S_4 in CSI topology which is in ON state.

The key waveforms of the VSI DPT are shown in Fig. 3(a). The double pulse of CSI DPT is the dual of VSI DPT, as shown in Fig. 3(b). It can be observed that the switch S_{c3} is always ON, and the signal of S_{c1} is inverse in polarity from S_{v2} in Fig. 3(a). There are two conditions for CSI DPT, as shown in Fig 4, and the devices S_{c4} and D_{c4} are replaced by a short circuit. The first condition when S_{c1} is off and S_{c3} is on represents the active state of 3-phase CSI, as shown in Fig 4 (c). The second condition when S_{c1} is on represents the zero state of 3-phase CSI, as shown in Fig 4 (d). There are five intervals for CSI DPT, as explained below:

Interval 1 (prior to t_0,): Both S_{c1} and S_{c3} are turned on. In this initial interval, there is no voltage across the output capacitor. All of the currents are flowing through S_{c1}, while there is no current through S_{c3}.

Interval 2 (from t_0 to t_1): In this interval, S_{c1} is turned off. S_{c3} and D_{c3} conducts the current I_{dc} in the forward direction in order to charge the capacitor to the desired voltage, as shown in Fig. 4 (a).

Interval 3 (from t_1 to t_2): At t_1, S_{c1} is turned on, and the current in the loop is commutated from S_{c3} to S_{c1} (Fig. 4(a) to (b)), which represents the real commutation of the three-phase CSI from active state to zero state (Fig. 4(c) to (d)). The S_{c1} turn-on transients can be evaluated. Since S_{c1} is always ON, the diode D_{c3} becomes reversed biased by the capacitor voltage. Thus, the capacitor is open-circuited and no longer charged. It should be mentioned that this interval should be short to minimize the voltage drop of the output capacitor due to any parasitic current, but long enough to stabilize the switching transients.

Interval 4 (from t_2 to t_3): At t_2, S_{c1} is turned off again. The current I_{dc} is commutated from S_{c1} to S_{c3} (Fig. 4(b) to (a)), which represents the commutation of the three-phase CSI from zero state to active state (Fig. 4(d) to (c)). The S_{c1} turn-off transition can be evaluated. This interval should also be short to avoid further charging of the capacitor, but long enough to stabilize the switching transients [10].

Interval 5 (from t_3 to end): From t_3, S_{c1} turns on, which is the last interval of the CSI DPT. The external switch is turned on, so that the resistor is connected in parallel with the capacitor to discharge.

III. Power Device Characterization Using CSI DPT

The CSI DPT circuits have been built to experimentally characterize the switching characteristics of the SiC MOSFET and SiC Schottky diodes. A single CSI switch includes 3 paralleled discrete SiC MOSFETs (C3M0016120K from CREE) and 3 paralleled SiC Schottky diodes (GC50MPS12-247 from GeneSiC) in series with the MOSFETs to handle the

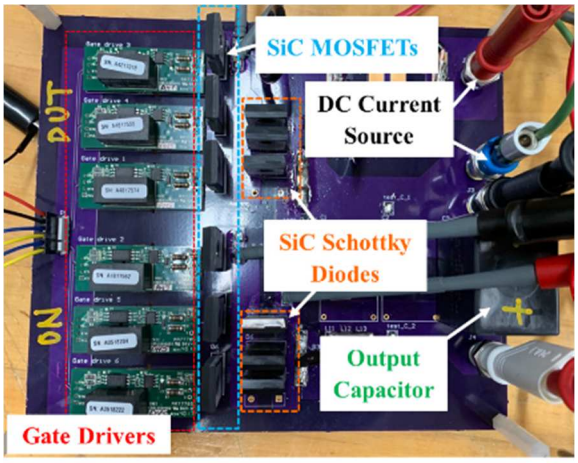

Fig. 5. CSI DPT prototype for power devices characterization

current required for this traction drive application, as shown in Fig. 5. The measured CSI DPT experimental test results for the operating point with 15A current for each device and a capacitor voltage of 250 V are shown in Fig. 6.

The turn-on and turn-off switching waveforms of the SiC MOSFET S_{c1} with a 10 Ω turn-on resistance in the gate drive are shown in Fig. 6(a) and (b). It can be observed that the rise time of SiC MOSFET is 46.4 ns, and the fall time is 31.2 ns at the 15 A, 250V operating point. The current resonance during the SiC MOSFET turn-on transient has little effect on the turn-on energy loss of the SiC MOSFET. The SiC MOSFET turn-on and turn-off instantaneous power with 10 Ω turn-on resistance are provided in Fig. 6(c) and (d). The peak instantaneous power values of 0.95 kW and 1.38 kW are dissipated in the MOSFET during turn-on and turn-off, respectively. Based on the SiC MOSFET instantaneous power, the turn-on energy is calculated to be 0.0476 mJ, and the turn-off energy is 0.0396 mJ. In addition, the temperatures of devices are recorded by the thermal camera. Fig. 7 shows the temperature of the paralleled device topology during 250V 15A steady-state operation without any forced cooling. The SiC Schottky diodes have the highest temperature of 92.8℃ at the operation point. The on-state resistance of the SiC MOSFET and SiC Schottky diode and forward voltage of the diode are measured at the operating condition, as shown in TABLE I.

TABLE I
MEASURED ON-STATE RESISTANCE AND FORWARD VOLTAGE OF SIC MOSFET AND SCHOTTKY DIODE

	On-state resistance (mΩ)	Built-in voltage drop (V)
SiC MOSFET	19.7	-
SiC Schottky diode	17.5	0.866

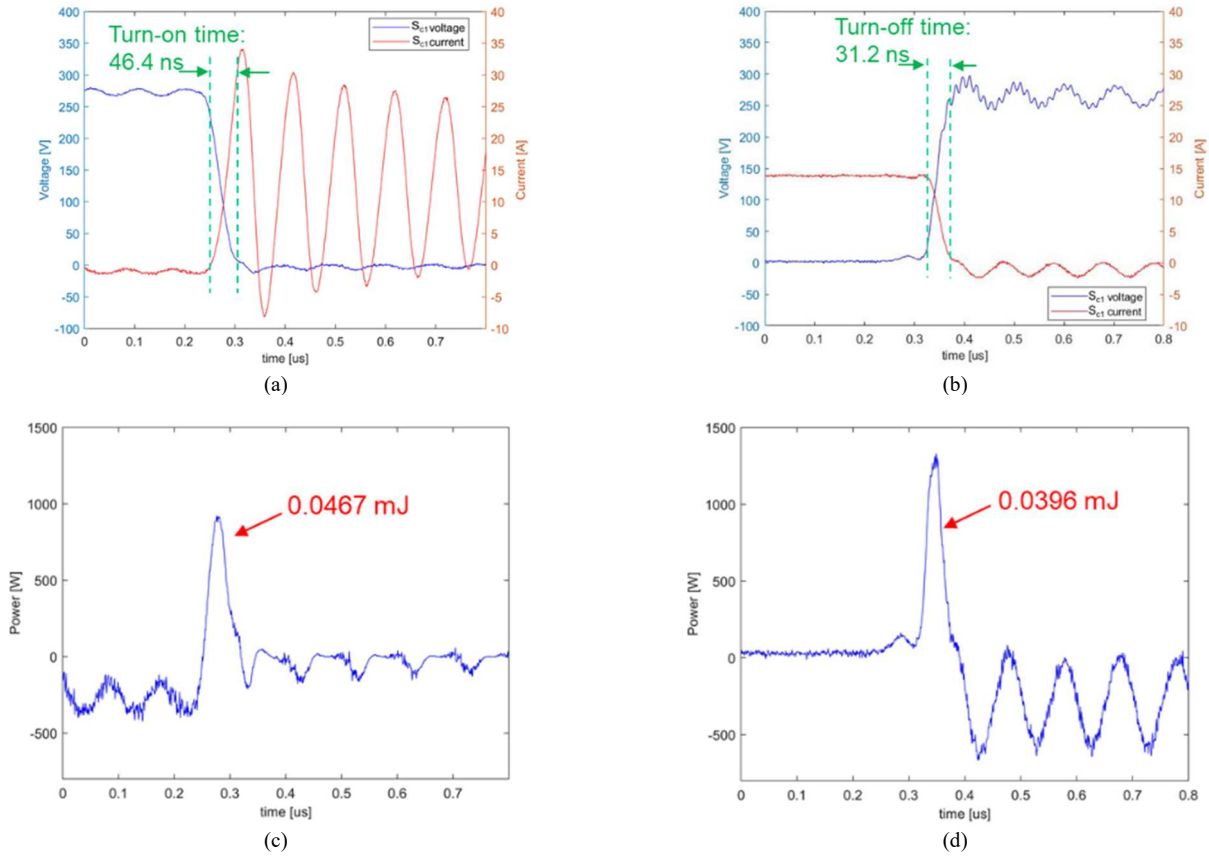

(a) (b) (c) (d)

Fig. 6. (a) Measured SiC MOSFET turn-on waveform; (b) Measured SiC MOSFET turn-off waveform; (c) Measured SiC MOSFET turn-on instantaneous power; (d) Measured SiC MOSFET turn-off instantaneous power.

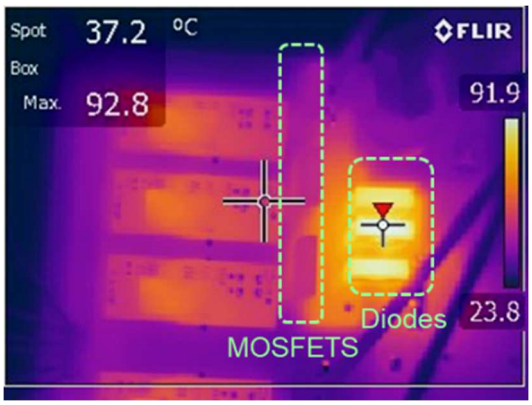

Fig. 7. Measured thermal results without cooling

IV. CSI Power Loss Modle

The power loss of CSI consists of the switching loss and conduction loss in the SiC MOSFET, and conduction loss in the Schottky diode [7]. The Schottky diode switching loss is very small as the SiC Schottky diode has almost zero reverse recovery current. Thus, the diode switching loss is neglected in this analysis.

The total switching loss of the SiC MOSFETs in the CSI considering temperature effects is estimated as [11,12]

$$P_{sw\_MOSFET} = \frac{3f_s}{\pi}\left(E_{on}(T_S) + E_{off}(T_S)\right)\frac{V_{llpk}I_{dc}}{V_{ref}I_{ref}} \quad (1)$$

where $E_{on}(T_S)$ and $E_{off}(T_S)$ are the measured turn-on and turn-off energy, respectively, at the condition of the reference voltage V_{ref} and reference current I_{ref}, taking thermal effects into account. T_S is the junction temperature of SiC MOSFET, I_{dc} is the dc-link current of CSI, as shwon in Fig. 1, and f_s is the switching frequency of the SiC MOSFET.

The total conduction loss of the SiC MOSFETs in CSI is given as

$$P_{c\_MOSFET} = 2{I_{dc}}^2 r_{DS(on)}(T_S) \quad (2)$$

where $r_{DS(on)}(T_S)$ is the temperature-dependent drain-source on-state resistance of the SiC MOSFET.

The total conduction loss of the SiC Schottky diodes can be represented by the following equations

$$P_{c\_diode} = 2I_{dc}(I_{dc}r_d(T_D) + V_F(T_D)) \quad (3)$$

where T_D is the junction temperature of SiC Schottky diode, $r_d(T_D)$ and $V_F(T_D)$ are the temperature-dependent on-state resistance and forward voltage of the SiC Schottky diode, respectively, which can be calculated from [13].

$$r_d(T_D) = a \times {T_D}^2 + b \times T_D + c \quad (4)$$

$$V_F(T_D) = m \times T_D + n \quad (5)$$

where

$a = 2.38 \cdot 10^{-7}$ (Ω/℃²)

$b = 3.38 \cdot 10^{-5}$ (Ω/℃)

$c = 0.01$ (Ω)

$m = -0.00123$ (V/℃)

$n = 0.995$(V)

The inductor loss of the CSI includes the copper loss P_{cu} in the winding resistance, and the core loss P_{fe} due to the hysteresis and eddy current losses in the magnetic core [7]:

$$P_L = P_{cu} + P_{fe} \quad (6)$$

The inductor copper loss originates in the inductor winding resistance r_L, which is defined as

$$P_{cu} = {I_{dc}}^2 r_L \quad (7)$$

The core loss of the powered core material can be estimated in a simplified form as [14]

$$P_{fe} = k{f_s}^{(i)}{B_L}^{(j)}W_{tfe} \quad (8)$$

where B_L is the peak magnetic flux density in the inductor $[T]$, W_{tfe} is the core weight $[kg]$, and k, m, n are the provided coefficients that vary with different core materials. For High Flux 60 powder cores, $k = 2.03 \times 10^{-7}$ $[\frac{s}{T \cdot kg}]$, $i = 1.23$, and $j = 2.56$.

The total loss of CSI is represented as equation (9) by combining all the loss components:

$$P_{CSI} = P_{sw} + P_{c\_MOSFET} + P_{c\_diode} + P_L \quad (9)$$

The estimated CSI loss and efficiency based on the CSI DPT measurement results and the CSI loss model are shown in TABLE II. Those estimates are based on the operation point of 55kW. The dc-link voltage is 650V, the dc-link current is 115A, and the switching frequency of the CSI is 50 kHz. The conduction and switching losses for SiC MOSFETs and SiC Schottky diodes are extrapolated to 120℃ from the measured temperatures. The results in this table indicate that the estimated loss of CSI is 1096.6 W, and the efficiency of the CSI is 98.04% at 55 kW operating point.

TABLE II. TOTAL CSI LOSS ESTIMATION BASED ON CSI DPT RESULTS AT 55 KW OPERATING POINT

	Parameter	Loss (W)
CSI	MOSFET switching loss	177.0
	MOSFET conduction loss	200.8
	Diode conduction loss	306.8
	Inductor loss	412
	Total CSI loss	**1096.6**
	Efficiency	**98.04%**

V. Conclusion

This paper has presented a laboratory demonstration of a promising CSI double-pulse test method [10] which is appropriate for normal operation of a CSI. The characteristics of the SiC MOSFET and in-series SiC Schottky diode used in a 55 kW (cont.) CSI have been measured using this CSI DPT technique. Models of the switching and conduction losses of the SiC MOSFET and the conduction losses of the SiC Schottky diodes have been derived from the CSI DPT measurement results. The estimated efficiency of the 55 kW CSI based on the CSI DPT measurement results is 98.04% for rated continuous power delivery.

Acknowledgment

This material is based upon work supported by the U.S. Department of Energy's Office of Energy Efficiency and Renewable Energy (EERE) under the Vehicle Technologies Office (VTO), Award Number DE-EE0008704, and the Advanced Research Projects Agency-Energy (ARPA-E), U.S. Department of Energy, under Award Number DE-AR0000893. The views and opinions of authors expressed herein do not necessarily state or reflect those of the United States Government or any agency thereof. The authors also gratefully acknowledge the support of the Wisconsin Electric Machines and Power Electronics Consortium (WEMPEC) including access to its laboratory facilities.

References

[1] Y. Nakakohara, H. Otake, T. M. Evans, T. Yoshida, M. Tsuruya, and K. Nakahara, "Three-phase LLC series resonant dc/dc converter using SiC MOSFETs to realize high-voltage and high-frequency operation," in *IEEE Transactions on Industrial Electronics*, vol. 63, no. 4, pp. 2103-2110, April 2016.

[2] E. A. Jones, F. F. Wang, and D. Costinett, "Review of commercial GaN power devices and GaN-based converter design challenges," in *IEEE Journal of Emerging and Selected Topics in Power Electronics*, vol. 4, no. 3, pp. 707-719, Sept. 2016.

[3] H. Ding, Y. Li, D. Han, M. Liu and B. Sarlioglu, "Design of a novel integrated motor-compressor machine with GaN-based inverters," in *Proc. 2017 19th European Conference on Power Electronics and Applications (EPE'17 ECCE Europe),* 2017, pp. P.1-P.9

[4] H. Dai and T. M. Jahns, "Comparative investigation of PWM current source inverters for future machine drives using high-frequency wide bandgap power switches," in *Proc. 2018 IEEE Applied Power Electronics Conference and Expo (APEC),* San Antonio, TX, 2018, pp. 2601-2608.

[5] F. Chen, H. Ding, S. Lee, W. Feng, T. M. Jahns, and B. Sarlioglu, "Current source inverter based large constant power speed ratio SPM machine drive for traction applications," in *Proc. 2020 IEEE Transportation Electrification Conference & Expo (ITEC),* Chicago, IL, USA, 2020, pp. 216-221.

[6] H. Umeda et al., "High power 3-phase to 3-phase matrix converter using dual-gate GaN bidirectional switches," in *Proc. IEEE Applied Power Electronics Conf. and Expo. (APEC), San Antonio*, TX, 2018, pp. 894–897

[7] F. Chen, W. Feng, H. Ding, S. Lee, T. M. Jahns and B. Sarlioglu, "Comprehensive efficiency analysis of current source inverter based SPM machine drive system for traction applications," in *Proc. 2020 IEEE Energy Conversion Congress and Exposition (ECCE),* Detroit, MI, USA, 2020, pp. 3002-3009.

[8] X. Ding, F. Chen, M. Du, H. Guo, and S Ren, "Effects of silicon carbide MOSFETs on the efficiency and power quality of a microgrid-connected inverter," in *Applied Energy*, 2016, 201: 270-283.

[9] H. Dai, R. A. Torres, T. M. Jahns and B. Sarlioglu, "Characterization and implementation of hybrid reverse-voltage-blocking and bidirectional switches using WBG devices in emerging motor drive applications," in *Proc. 2019 IEEE Applied Power Electronics Conference and Exposition (APEC),* Anaheim, CA, USA, 2019, pp. 297-304.

[10] R. A. Torres, H. Dai, T. M. Jahns and B. Sarlioglu, "Operation and Analysis of current-source inverters using dual-gate four-quadrant wide-bandgap power switches," in *Proc. 2019 IEEE Energy Conversion Congress and Exposition (ECCE),* Baltimore, MD, USA, 2019, pp. 2353-2360.

[11] G. Su and P. Ning, "Loss modeling and comparison of VSI and RB-IGBT based CSI in traction drive applications," in *Proc. IEEE Transportation Electrification Conference and Expo (ITEC),* Detroit, MI, 2013, pp. 1-7.

[12] M. H. Bierhoff and F. W. Fuchs, "Semiconductor losses in voltage source and current source IGBT converters based on analytical derivation," in *Proc. 2004 IEEE 35th Annual Power Electronics Specialists Conference*, 2004, pp. 2836-2842 Vol.4.

[13] http://www.genesicsemi.com/sic-schottky-mps/GC50MPS12-247/GC50MPS12-247.pdf

[14] Wm. T. McLyman, Transformer and inductor design handbook, 3rd ed., Marcel Dekker, Inc., 2004, pp. 72-76.